



A biophysical and structural study of two chitinases from *Agave tequilana* and their potential role as defense proteins

Yusvel Sierra-Gómez¹, Annia Rodríguez-Hernández¹, Patricia Cano-Sánchez¹, Homero Gómez-Velasco¹, Alejandra Hernández-Santoyo¹, Dritan Siliqi²  and Adela Rodríguez-Romero¹ 

¹ Instituto de Química, Universidad Nacional Autónoma de México, Ciudad de México, Mexico

² Istituto di Cristallografia, Consiglio Nazionale delle Ricerche, Bari, Italy

Keywords

Agave tequilana; antifungal proteins; binding energetics; class I chitinases; SAXS models

Correspondence

A. Rodríguez-Romero, Instituto de Química, Universidad Nacional Autónoma de México, Circuito Exterior, Ciudad Universitaria, Coyoacán, Ciudad de México 04510, Mexico

Tel: +5255 56224568

E-mail: adela@unam.mx

(Received 21 December 2018, revised 4 May 2019, accepted 8 July 2019)

doi:10.1111/febs.14993

Plant chitinases are enzymes that have several functions, including providing protection against pathogens. *Agave tequilana* is an economically important plant that is poorly studied. Here, we identified a chitinase from short reads of the *A. tequilana* transcriptome (AtChi1). A second chitinase, differing by only six residues from the first, was isolated from total RNA of plants infected with *Fusarium oxysporum* (AtChi2). Both enzymes were overexpressed in *Escherichia coli* and analysis of their sequences indicated that they belong to the class I glycoside hydrolase family19, whose members exhibit two domains: a carbohydrate-binding module and a catalytic domain, connected by a flexible linker. Activity assays and thermal shift experiments demonstrated that the recombinant *Agave* enzymes are highly thermostable acidic endochitinases with T_m values of 75 °C and 71 °C. Both exhibit a molecular mass close to 32 kDa, as determined by MALDI-TOF, and experimental pI's of 3.7 and 3.9. Coupling small-angle x-ray scattering information with homology modeling and docking simulations allowed us to structurally characterize both chitinases, which notably show different interactions in the binding groove. Even when the six different amino acids are all exposed to solvent in the loops located near the linker and opposite to the binding site, they confer distinct kinetic parameters against colloidal chitin and similar affinity for (GlnNAc)₆, as shown by isothermal titration calorimetry. Interestingly, binding is more enthalpy-driven for AtChi2. Whereas the physiological role of these chitinases remains unknown, we demonstrate that they exhibit important antifungal activity against chitin-rich fungi such as *Aspergillus* sp.

Database

SAXS structural data are available in the SASBDB database with accession numbers SASDDE7 and SASDDA6.

Enzymes

Chitinases (EC 3.2.1.14).

Abbreviations

(GlcNAc)₆, chitohexaose; CatD, catalytic domain; CBM, carbohydrate-binding module; CD, circular dichroism; DLS, dynamic light scattering; GH, glycoside hydrolase; GlcNAc, *N*-acetylglucosamine; ITC, isothermal titration calorimetry; MALDI-TOF, matrix-assisted laser desorption/ionization-time of flight; NMR, nuclear magnetic resonance; PR, pathogenesis-related; SAXS, small-angle x-ray scattering; SEC, size-exclusion chromatography; T_m , melting temperature.

Introduction

Chitinases (EC 3.2.1.14) are enzymes that hydrolyze β -1,4-bonds between *N*-acetylglucosamine (GlcNAc) residues in chitin ($C_8H_{13}NO_5$)_{*n*}, which is present in the cell walls of fungi, the exoskeleton of most insects, in yeasts, algae, and the shells of crustaceans, among others [1]. This type of enzymes is involved in numerous physiological events such as abiotic stress responses [2], including antifungal activity versus pathological fungus [3,4]. The Carbohydrate-Active Enzyme (CAZy) database classifies most chitinases in the glycosyl hydrolase (GH) families 18, 19 based on primary sequence, three-dimensional structure, and catalytic mechanism [5]. Those belonging to the GH18 family are found in most organisms, whereas the ones in the GH19 family have been detected mainly in plants as part of the defense mechanism against pathogens. Chitinases of the GH19 family consist of two domains, the N-terminal carbohydrate-binding module (CBM18) and a catalytic domain (CatD) that exhibits an α -helix rich/lysozyme-like structure with diverse loop arrangements and they hydrolyze their substrates through a single-displacement mechanism with inversion of the anomeric carbon configuration [6].

Plant chitinases are further classified into seven classes (I–VII) [7–11]. Classes I, II, IV, VI, and VII belong to the GH19 family, whereas classes III and V are grouped in the GH18 family [12]. In class I chitinases, the CatD and CBM18 domains are connected by a flexible linker that varies in length and amino acid composition [9]. The CBM18, or hevein-like domain, is also present in class IV but is absent in class II chitinases [7]. Several studies indicate that one plant can possess numerous chitinases belonging to different classes, or several isoforms with redundant functions in order to guarantee the accomplishment of the biological function [12–15].

Most investigations into the structure–function relationships of plant chitinases, belonging to classes I and IV, have been carried out on empty catalytic domains or in complex with GlcNAc oligosaccharides of up to six units [16,17]. However, for enzymes in class I, it has not been possible to obtain a full-length crystallographic structure due to the flexibility of the linker that binds the two domains. There is only one report in which both domains, without the linker, are observed in the crystal structure (PDB entry 2DKV) [18]. These domains seem to contribute differently to the activity of class I chitinases, even in defense-related functions [4,15]. Therefore, it is interesting to perform studies that provide information regarding the spatial distribution of both domains and its importance in the

activity and kinetic properties of class I chitinases. The structural characterization of chitinases from plants may lead to the development of new chimeric enzymes that could be used to obtain varieties that are more resistant to pathogens [19].

While many chitinases are known to be important in numerous plants, none have been isolated from the genus *Agave*. There are only four enzymes that have been identified in the transcriptome of this plant, and they were isolated and characterized from total RNA: two fructosyltransferases (1-SST and 6G-FFT) and two types of invertases (cell wall and vacuolar) [20]. *Agaves* are succulent monocotyledonous plants native to deserts or moderately dried environments of North America. The genus *Agave* is cultivated to produce fiber, food, beverages, fuel, etc., and has great socio-economic and agroecological value, especially in hot and drought-prone regions of the world; despite its adaptability, these plants suffer from diseases, such as those caused by insects and fungus. Within this genus, *Agave tequilana* is primarily used for the elaboration of beverages, in soil conservation; furthermore, it has also been indicated that this plant can potentially be an important source of lignocellulosic bioenergy feedstocks [21–23].

Here we describe the overexpression, catalytic activity, and binding affinity determinations, as well as a structural characterization in solution of two novel class I chitinases, present in *A. tequilana*. Isothermal titration calorimetry (ITC) using chitohexaose (GlcNAc)₆ and the active enzymes, under very low activity conditions (pH 7.0, 18 °C), allowed us to determine the K_d and the associated thermodynamic parameters. The structural characterization of both chitinases by means of small-angle x-ray scattering (SAXS) analysis and homology modeling showed subtle differences between them. Docking simulations using (GlcNAc)₆ revealed slightly different binding grooves. Finally, these enzymes were found to be highly thermostable and exhibited antifungal activity versus *Aspergillus* sp., implying that they could exert a protective role in the plant.

Results

Class I chitinases obtained from the transcriptome and the cDNA of *Agave tequilana* plants

A class I chitinase from *A. tequilana* was assembled from transcriptome short readings. The whole gene was assembled and submitted for a nucleotide BLAST

alignment using the NCBI server [24], which confirmed that it corresponded to a class I chitinase. The sequence obtained (named AtChi1) corresponds to a class I chitinase that exhibits more than 66% sequence identity with chitinases from *Poa pratensis*, *Ananas comosus*, *Zea mays*, and *Oryza sativa*. The gene identified encodes for a protein of 324 residues, including a signal peptide of 20 residues at the N terminus (Fig. S1). According to the predictions of servers SignalP (<http://www.cbs.dtu.dk/services/SignalP/>) [25] and Phobius (<http://phobius.sbc.su.se/>) [26], the first 60 base pairs encode for a signal peptide for secretion. After the signal peptide, residues 1–39 correspond to the CBM18 present in class I plant chitinases that shows a hevein-like fold [27,28]. Residues Gly40 to Ser66 form the interdomain flexible linker (shown in yellow in Fig. 1A) that connects the CBM18 with the C-terminal CatD.

Moreover, a cDNA fragment encoding an *A. tequilana* class I chitinase that lacks a signal peptide was amplified from total RNA of *Fusarium oxysporum* infected leaves using RT-PCR. The PCR products obtained from infected leaves were subjected to agarose gel electrophoresis; and from leaves with 4 weeks

of infection, three bands of approximately 900, 1000, and 1200 bp were identified (Fig. 1B). However, from the leaves with 7 weeks of infection, only the 900 bp band was still visible. This band was isolated, cloned and expressed (AtChi2) (Fig. 1B). The latter has only six residues different from those in AtChi1 (shown in green in Fig. 1A) but conserves the putative catalytic acidic residues, Glu129 and Glu151, that have been described for other plant class I chitinases (shown in magenta) (Fig. 1A) [18,29].

Characterization of the purified AtChi1 and AtChi2

Both chitinases were purified from 16 h cell cultures of Rosetta Gami and SHuffle strains, respectively. These strains were selected because they allow the correct formation of disulfide bonds, of which class I plant chitinases usually have more than six (three in the catalytic domain and four in the CBM18). The protocol used allowed us to obtain the two enzymes with a high degree of homogeneity, appearing as single bands on SDS/PAGE gels near 31 kDa (Fig. 2A). Recombinant AtChi1 and AtChi2 were purified with yields of 4 and

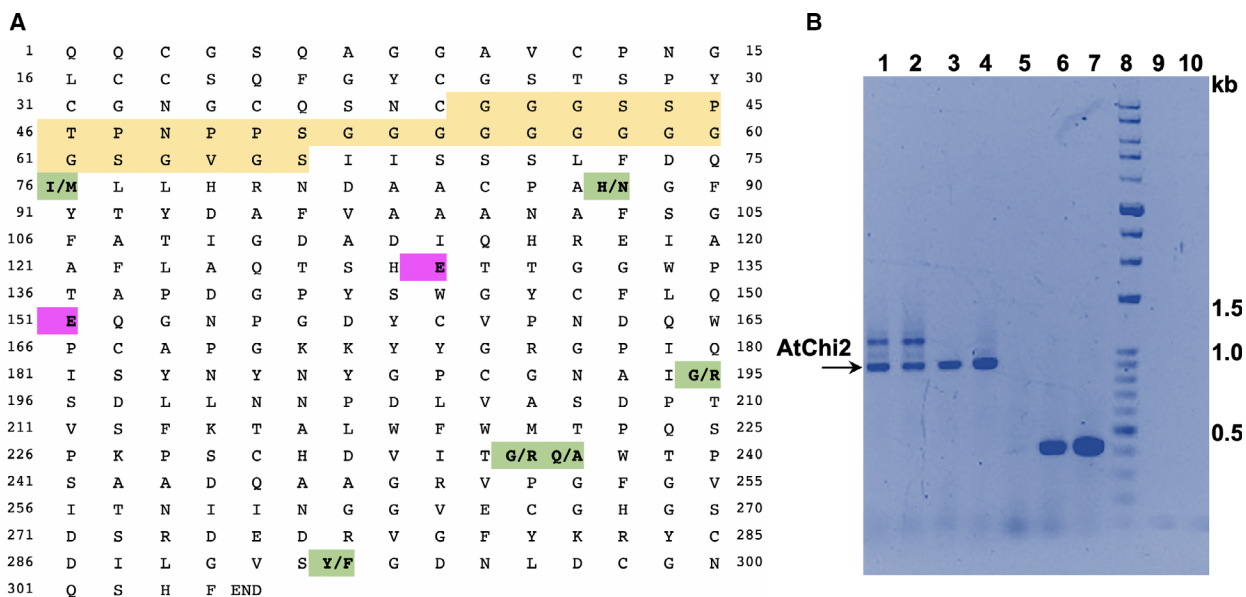


Fig. 1. Amino acid sequences of chitinases from *Agave tequilana*. (A) Sequence comparison between AtChi1 assembled from short reads of *A. tequilana* transcriptome and AtChi2 isolated from infected plant total RNA. Mature AtChi1 comprises residues Gln1 to Cys39 that correspond to the CBM18, the linker between the CBM18 and the catalytic domain shown in yellow (residues Gly40–Ser66), and the catalytic domain (residues Ile67–Phe304). Residues in green show the differences between the two isoforms, which are present in the catalytic domain. Residues shown in purple are the catalytic Glu129 and Glu151. (B) Agarose gel showing the AtChi2 gene from infected leaves total RNA (*A. tequilana* plants after 4 and 7 weeks of infection with *Fusarium oxysporum*). Lane 1: Big leaves (BL), 4 weeks after infection; Lane 2: Small leaves (SL), 4 weeks after infection; Lane 3: BL, 7 weeks after infection; Lane 4: SL, 7 weeks after infection; Lane 5: Negative control without polymerase; Lane 6: PCR positive control, BL-400 bp fragment of glyceraldehyde dehydrogenase (GDH); Lane 7: SL-GDH; Lane 8: 1 kb molecular weight ladder; Lane 9: BL without infection. Lane 10: SL without infection.

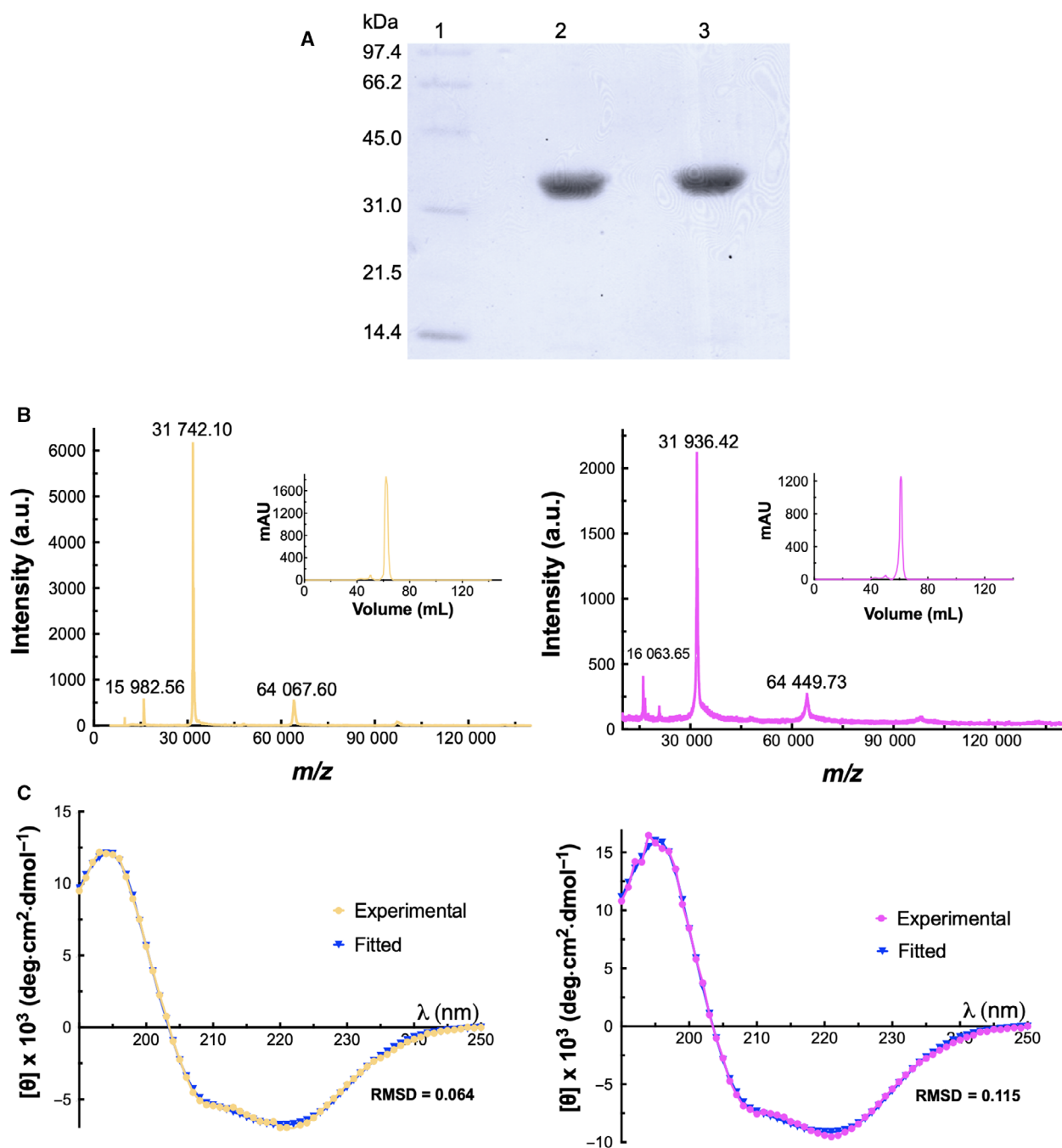


Fig. 2. Purification, mass determination, and folding analysis of AtChi1 and AtChi2. AtChi1: left side (yellow) and AtChi2: right side (purple). (A) SDS/PAGE of the purified enzymes: Lane 1, molecular weight size markers (kDa); Lane 2, AtChi1, Lane 3 AtChi2. (B) MALDI-TOF spectra for both enzymes; insets correspond to the SEC elution profile of the pure enzymes. (C) CD spectra in the far-UV region. [AtChi1] = 0.186 mg·mL⁻¹, [AtChi2] = 0.23 mg·mL⁻¹.

2 mg·L⁻¹ of culture, respectively. The mature AtChi1 has 304 residues, including 17 cysteines in conserved positions of the class I chitinases family, with a theoretical molecular mass of 31.7 kDa and pI of 4.7.

AtChi2 is a protein of 304 residues that also exhibits the conserved cysteine positions and has a theoretical molecular mass of 31.9 kDa and pI of 4.82. These theoretical masses were calculated for the recombinant

proteins with three additional residues at the N terminus due to the cleavage site for TEV, Gly-Gly-Ala for AtChi1 and Ser-Asn-Ala for AtChi2. The masses of the two proteins were confirmed by MALDI-TOF spectrometry (Fig. 2B) with base m/z peaks of 31.7 and 31.9 kDa, and the experimental pIs were 3.7 and 3.9, respectively.

Furthermore, the far-UV circular dichroism (CD) spectra of both enzymes were very similar and exhibited a clear helical character (Fig. 2C) with two negative peaks at 222 and 208 nm. However, the analysis indicated a high contribution of loops and flexible regions. The BeStSel server estimated equivalent amounts of α -helices and β -sheets, 24.4% and 23.5%, respectively for AtChi1, whereas for AtChi2 these values were 31.3% and 15%, respectively. It is important to note that this server predicted a high content of turns and other disordered structures for both enzymes: 52.2% for AtChi1 and 53.6% for AtChi2, results that are in agreement with the presence of loops and flexible regions common in 'loopful' plant class I chitinases (Fig. 2C) [17,18,30,31].

Notably, both chitinases only exhibited important activity over insoluble colloidal chitin, two orders of magnitude higher than the activity observed when the oligosaccharides chitohexaose (GlnNac)₆ and chitotriose (GlnNac)₃ were used under the same conditions (Fig. S2). No activity was detected with 4-Methylumbelliferyl *N*-acetyl- β -D-glucosaminide and 4-Methylumbelliferyl *N,N'*-diacetyl- β -D-chitobioside. The effect of pH on the stability of the two chitinases was measured using different buffers, ranging in pH from 2.0 to 10.0. As shown in Fig. 3A, both chitinases were optimally active at pH 5.0 (37 °C) using colloidal chitin as substrate. Moreover, both enzymes were stable over the pH range 3–10, retaining more than 75% of its activity even after incubation for 48 h at these pH values. Furthermore, the activities of the two chitinases were evaluated on colloidal chitin and data of initial rates versus substrate concentration were adjusted to a Michaelis–Menten plot and kinetic parameters were calculated (Fig. 3B). For AtChi1, $K_m = 4.84 \pm 0.45 \text{ mg}\cdot\text{mL}^{-1}$, $k_{\text{cat}} = 0.47 \pm 0.11 \text{ min}^{-1}$, and $k_{\text{cat}}/K_m = 9.7 \times 10^{-2} \text{ mL}\cdot\text{mg}^{-1}\cdot\text{min}^{-1}$ at the conditions described in the Materials and methods section, whereas for AtChi2 $K_m = 8.01 \pm 0.67 \text{ mg}\cdot\text{mL}^{-1}$, $k_{\text{cat}} = 0.53 \pm 0.09 \text{ min}^{-1}$, and $k_{\text{cat}}/K_m = 6.6 \times 10^{-2} \text{ mL}\cdot\text{mg}^{-1}\cdot\text{min}^{-1}$ in the same conditions (Fig. 3B), indicating a higher affinity and catalytic efficiency for AtChi1.

Analysis of thermal shift assays for the two chitinases indicated the higher melting temperatures (T_m) in pH values between 6.0 and 6.5 (Fig. 3C). The maximum T_m values were 75 °C and 71 °C for AtChi1 and

AtChi2, respectively. For this reason, we selected MES pH 6.0 as the condition of maximum stability.

Binding affinity and thermodynamic characterization

To measure the binding affinities between the two chitinases and chitohexaose, we performed ITC experiments and determined the equilibrium dissociation constant (K_d). Both enzymes bound chitohexaose with a stoichiometry of $n = 1$ and K_d values of 208 and 128 μM , respectively (Fig. 4A,B). These K_d values were consistent with the binding affinities reported for a class I GH19 chitinases from *Bryum coronatum* (moss) using ITC and GlcNac oligosaccharides [30]. Moreover, data showed a 1.5-fold difference in the enthalpy of formation for the chitohexaose–chitinase complex with a more negative value for AtChi1 $\Delta H = -8.6 \pm 0.1 \text{ kcal}\cdot\text{mol}^{-1}$ compared to $\Delta H = -5.5 \pm 0.0 \text{ kcal}\cdot\text{mol}^{-1}$ for the AtChi2. There is a 10-fold difference in entropy between the two enzymes with values of $-T\Delta S = 3.7 \pm 0.1 \text{ kcal}\cdot\text{mol}^{-1}$ for AtChi1 and $-T\Delta S = 0.3 \pm 0.0 \text{ kcal}\cdot\text{mol}^{-1}$ for AtChi2. It is important to mention that the activity of the two enzymes over chitohexaose was very low in the ITC assay conditions (pH 7.0, 18 °C), with a maximum 0.04% of the substrate consumed during the experiment.

Solution structure and homology modeling

We characterized the low-resolution overall shape and maximum particle size of the complete chitinases in solution using SAXS. Data collection and structural parameters for the experiments are reported in Table 1. Raw data for both enzymes, with insets of the Guinier plots, are shown in Fig. 5A. For AtChi1, we used the lowest protein concentration because we observed some aggregation during the experiment at higher concentrations. It is important to note that before the experiment both proteins were monodisperse and monomeric as confirmed by SEC (Fig. 2B, inset) and DLS (results not shown). For AtChi2 we used a merged file with the 7.5 and 3.75 $\text{mg}\cdot\text{mL}^{-1}$ concentrations for the analysis. All SAXS data are deposited in the SASBDB database [32] with IDs SASDDE7 and SASDDA6 for AtChi1 and AtChi2, respectively. The radius of gyration (R_g) determined for AtChi1 was $26.10 \pm 1.3 \text{ \AA}$, whereas for AtChi2 it was $24.1 \pm 0.47 \text{ \AA}$ (Fig. 5B). The Guinier plot reveals a linear fit suggesting that there are no inter-particle interactions at the concentration used for each protein. At this point, it is important to

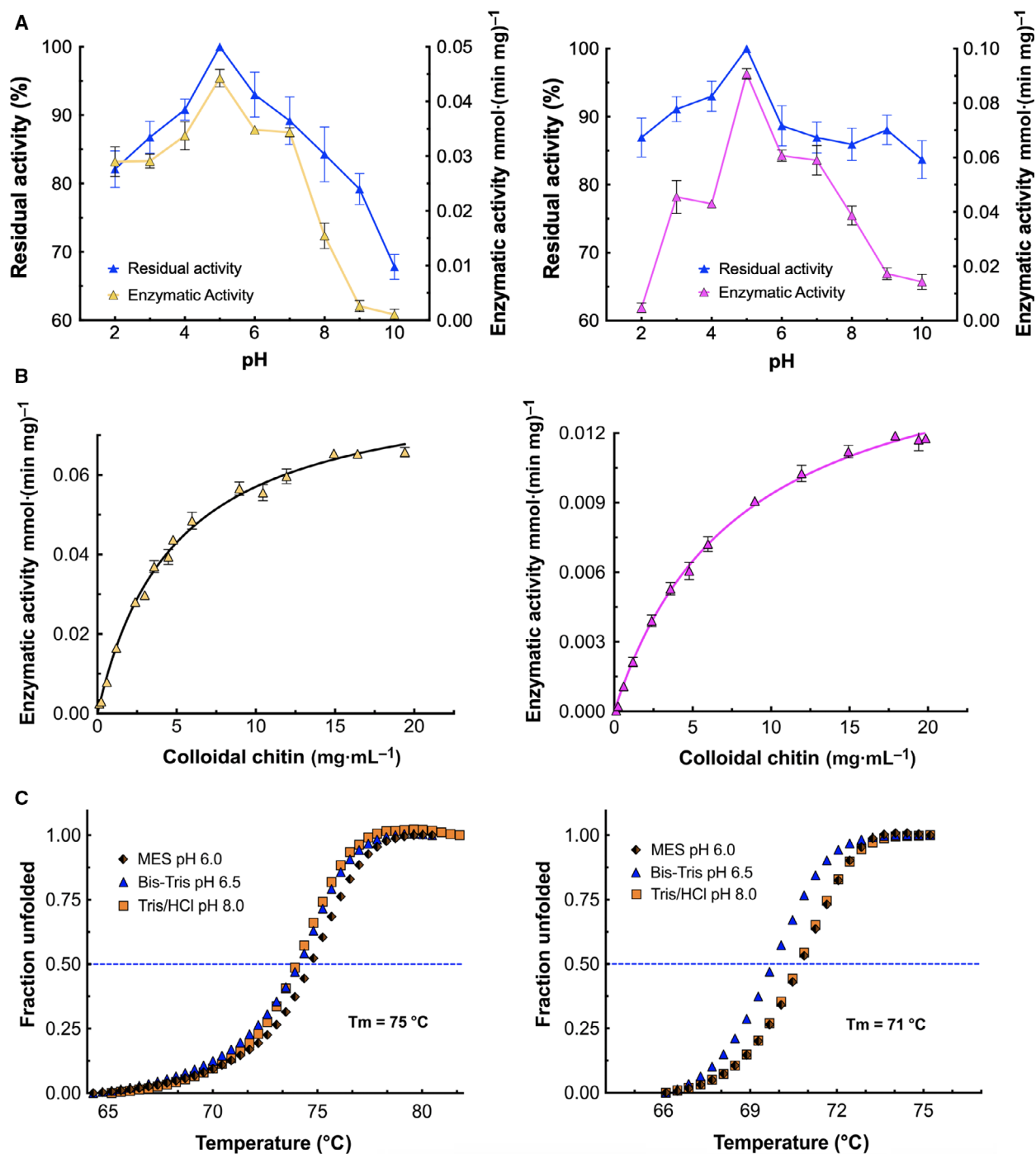


Fig. 3. Characterization of AtChi1 and AtChi2. AtChi1: yellow and AtChi2: purple. (A) Optimum pH for activity and stability (shown in blue) using colloidal chitin as substrate. [Colloidal chitin] = $4.78 \text{ mg} \cdot \text{mL}^{-1}$ (w/v). Assay conditions: for activity, 24 h at 37°C ; for stability, 48 h. (B) Michaelis–Menten curves obtained using the GRAPHPAD software. (C) Thermodynamic stabilities using Thermal Shift Assays. In (A) and (B), the data show the means of three independent experiments and bars indicate the standard deviations.

mention that the Guinier analysis from ATSAS only gives fidelity coefficients, not linear regression coefficients. The maximum particle dimensions, derived

from the distance distribution function $P(r)$, were 97.6 and 98 Å for AtChi1 and AtChi2, respectively (Fig. 5B).

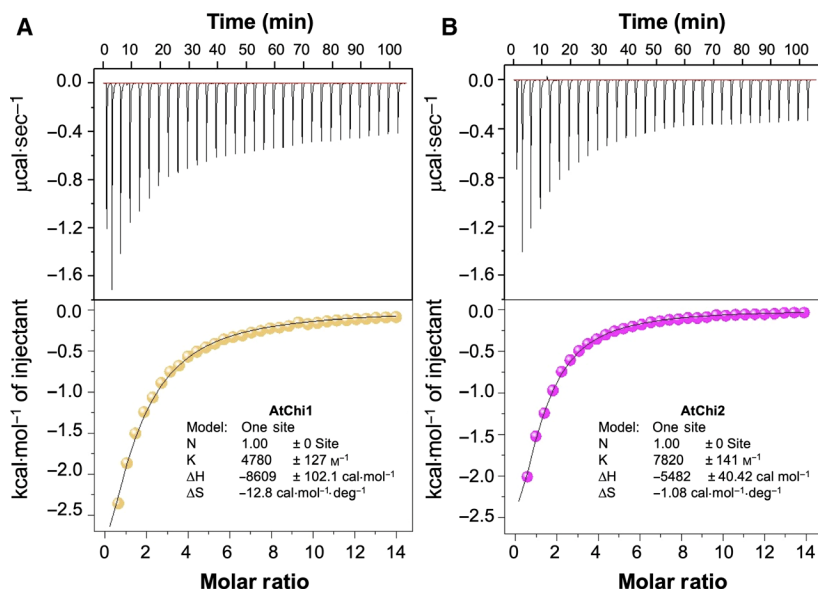


Fig. 4. ITC thermograms and theoretical fits for the binding of chitohexaose to AtChi1 (left) and AtChi2 (right). Titrations were conducted in 20 mM phosphate buffer pH 7.0 (18 °C). Thermodynamic parameters obtained from individual experiments are shown in boxes.

The *ab-initio* low-resolution molecular models of AtChi1 and AtChi2 in solution were generated using DAMMIF [33] and DAMFILT [34]. We also deposited the best model generated in DAMMIF for each enzyme in the SASBDB website. Both models clearly indicate the presence of two lobes that are joined by a hinge region that corresponds to the 27 amino acids linker (Fig. 5C). Three-dimensional models of AtChi1 and AtChi2 were generated with the Robetta server [35] that used the crystal structure of rice class I chitinase (PDB entry 2DKV) to model the CBM18 for both Agave enzymes. This structure lacks the linker between the catalytic domain and the CBM. The catalytic domains were modeled using the structure of the rye chitinase (PDB entry 4DWX) (identity 76.5%), that lacks the CBM18 and the linker. These AtChi1 and AtChi2 models showed 99.1% and 99.5% of the residues in the most favored region of the Ramachandran plot, respectively, and 0.9% and 0.5% in the disallowed regions of the Ramachandran plot, respectively [36]. For AtChi1, these residues correspond to Gln152 and Tyr 183, and for AtChi2 to Tyr 183, which are located in the chitin binding groove. Ramachandran outliers do happen in several enzymes and antibodies indicating strained conformations of residues in active or binding sites [37].

Robetta models were fitted to the experimental scattering curves from SAXS with the CRY SOL program [38]. The models for each enzyme with the best fitting to SAXS data were superimposed into the SAXS envelopes revealing good global fitting (Fig. 5C). For AtChi1 the chi-square goodness of fit for the three best Robetta models was: 4.09, 3.79, 4.03; and for AtChi2

Table 1. SAXS data collection and structural parameters

	AtChi1	AtChi2
Data collection parameters		
Detector	Rayonix MX225-HE	Pilatus3 X 1M
Defining slit size (<i>H</i> mm × <i>V</i> mm)	0.3 × 0.3	0.3 × 0.3
Detector distance (m)	1.78	1.80
Wavelength (Å)	1.127	1.127
Exposure time (s)	10 × 1	10 × 1
Protein concentration (mg·mL ⁻¹)	0.23–15	0.23–7.5
Temperature (K)	288	288
Structural parameters		
<i>R</i> _g from Guinier (nm)	2.6 ± 0.13	2.4 ± 0.047
<i>D</i> _{max} (nm)	9.7	9.8
Porod volume (nm ³)	52	49

these values were 2.44, 2.51 2.19. The best fitting for both enzymes is shown in Fig. 5C. The catalytic domains of both chitinases were almost identical with an RMSD of only 0.263 Å, while the linker and CBM18 exhibited slightly different conformations (Fig. 5D). It is important to mention that the best Robetta CatDs models were compared with the CatDs of plant class I chitinases deposited in the PDB and slight differences are observed in the longest loop (III), where Glu151 is located.

To get insight into the binding of chitohexaose, we used the homology models of the catalytic domains obtained using Robetta, which were fitted onto the SAXS experimental envelopes, with the lowest

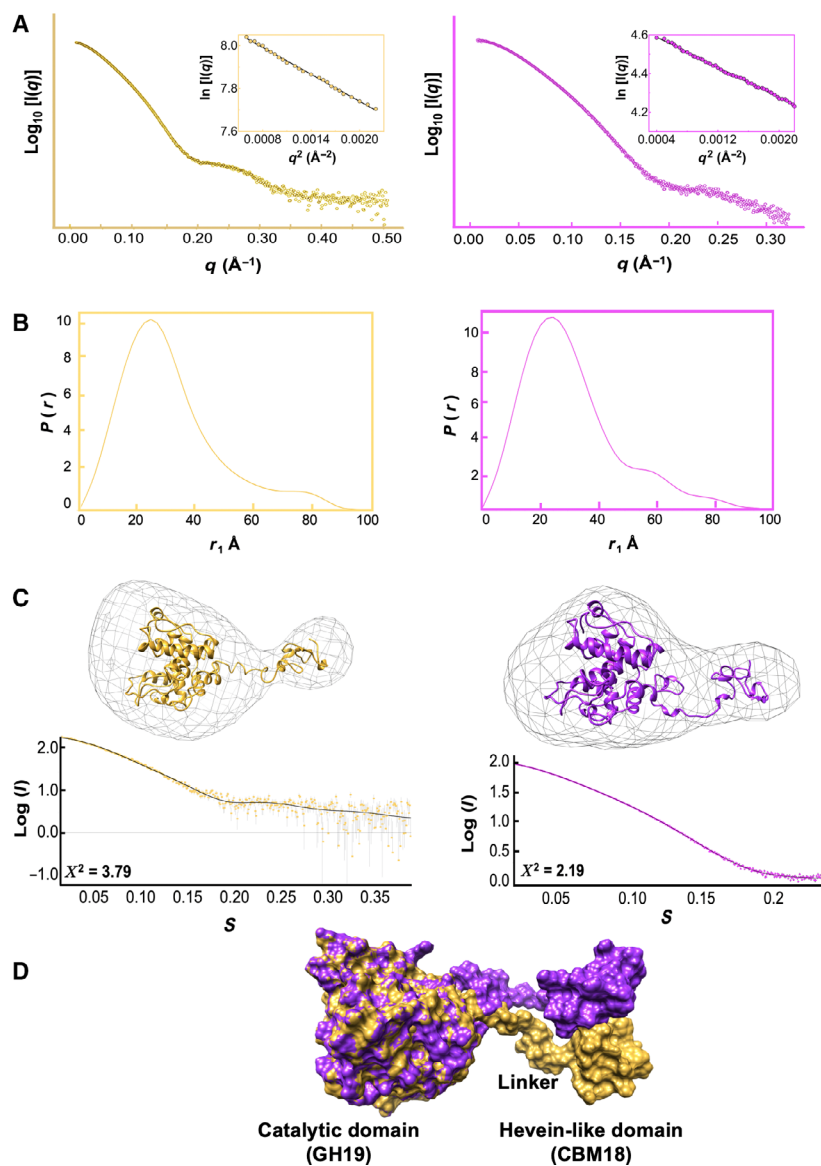


Fig. 5. SAXS analysis of AtChi1 (left) and AtChi2 (right). (A) Scattering experimental data with an inset of the Guinier plot. (B) Normalized inter-atomic pairwise distribution function $P(r)$. (C) Structural fitting of the Robetta models for AtChi1 (gold) and AtChi2 (purple) into the *ab initio* calculated SAXS envelopes. Lower panel shows simulated curves obtained with the *CRYSOLE* program [38]. Chi-squared values are indicated for both proteins (D) Superposition of the Robetta models for AtChi1 (gold) and AtChi2 (purple, in surface representation), which includes the CBM18 and the CatD.

chi-squared values. A superposition of these models showed RMSD values that varied from 0.08 Å (Model 1 versus Model 2) to 0.159 Å (Model 1 versus Model 5) for AtChi1, whereas for AtChi2 these values were 0.134–0.181 Å (Fig. S3). Docking experiments were performed allowing side-chain flexibility and even though the substrate binding clefts look almost identical to those in other plant chitinases, they showed slightly different binding energies ($\text{kcal}\cdot\text{mol}^{-1}$): -8.3 , -8.4 , -8.6 , -7.5 , -8.2 for the five AtChi1 dockings, whereas for AtChi2 these values were: -8.0 , -8.2 , -7.5 , -7.8 , -7.7 (Fig. S4). It is worth mentioning that the experimental ΔH values determined using ITC were $-8.609 \pm 0.1 \text{ kcal}\cdot\text{mol}^{-1}$ for AtChi1 compared to $-5.482 \pm 0.0 \text{ kcal}\cdot\text{mol}^{-1}$ for AtChi2, while ΔG

values were -4.56 and $-5.2 \text{ kcal}\cdot\text{mol}^{-1}$ for AtChi1 and AtChi2, respectively. The first five solutions of lower energy were selected and analyzed considering the previous reports on the amino acids involved in interactions with the substrates or products of active GH19 chitinases [16,17,29]. Figure 6B illustrates the interaction of the catalytic residues with $(\text{GlcNAc})_6$ when the latter was positioned throughout the groove in subsites -4 to $+2$. Figure 6C shows a surface view of the catalytic cleft of both enzymes with $(\text{GlcNAc})_6$. Interestingly, as shown in this figure the binding groove for AtChi2 is slightly wider than the one in AtChi1, and there are more interactions of AtChi1 with chitohexaose as estimated using CONTACT in ccp4 [39].

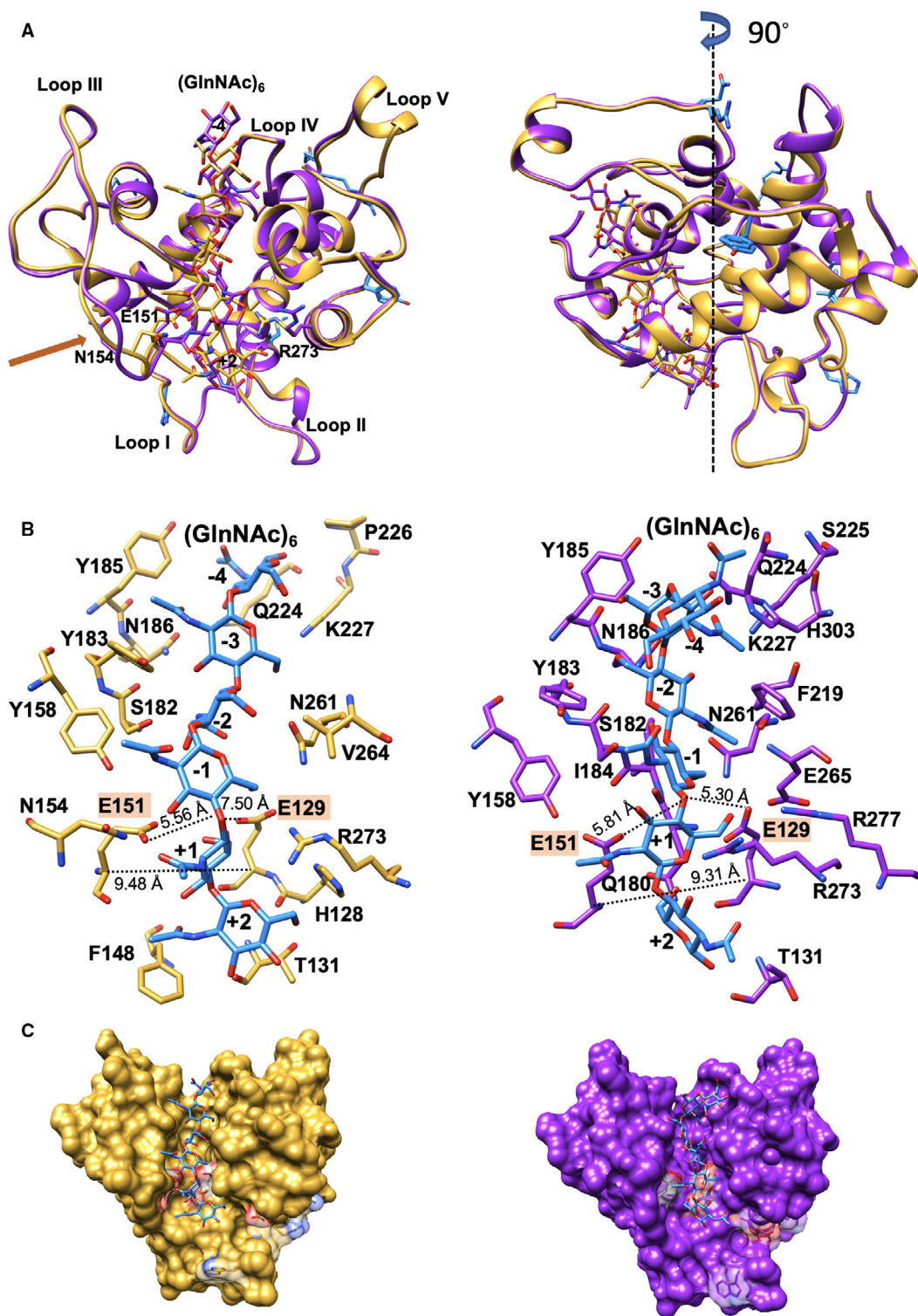


Fig. 6. Docking analyzes using (GlnNAc)₆ on AtChi1 and AtChi2 Robetta models. (A) Left side: Superposition of the catalytic domains showing the docked chitohexaose. The arrow indicates the slightly different conformation for loop III in both chitinases where the catalytic residue E151 is located. Right side: 90° view showing the six different residues in both enzymes as blue sticks. (B) Zoom of the groove where the residues that could be involved in the interaction with (GlnNAc)₆ are shown in AtChi1 (left) and AtChi2 (right). (C) Surface representation of the catalytic groove with the oligosaccharide. Residues in transparent areas (W134, D276, Y142, R283, Q75, K282) exhibit different conformation due to the six mutations between both chitinases. Colors are the same used in Fig. 5.

Antifungal activities versus phytopathogenic fungi

The antifungal activity of both chitinases versus the pathogenic fungi *Aspergillus* sp. is shown in Fig. 7. AtChi1 exhibited higher antifungal activity at both concentrations when compared with AtChi2 and fungal inhibition showed concentration dependence.

Discussion

Recently, the study of chitinases has been an important objective of numerous research projects due to their enormous potential applications, such as biocontrol agents, to develop pest-resistant species of economically important plants [40,41], or for their role as molecular markers of numerous diseases [42–44], and they are also attractive for protein engineering studies [45,46]. In the present study, the first chitinases from the genus *Agave* (AtChi1 and AtChi2) were produced in *E. coli* cells and the recombinant products were purified and characterized. The predicted AtChi1 was identified by inspecting the *Agave* transcriptome, and AtChi2 was amplified from infected leaves RNA using RT-PCR. Three PCR products were obtained after 4 weeks of infection and only one band was observed for the 7 weeks infected plant (Fig. 1B). These results suggest that during infection more isoforms could be expressed in the plant and that the chitinase genes respond differently to biotic stresses [47]. Both chitinases belong to the class I/GH19 family and exhibit only six different residues in their sequences (Fig. 1A), which notably are all exposed to the solvent and located near the hinge region and opposite to the binding groove. This result is interesting because it has

been reported that molecular evolution of class I chitinase is driven by selection for advantageous mutations, causing an excess of amino acid replacements in the active site and substrate binding cleft [48], which is not the case.

Plant chitinases are either induced as PR proteins in response to insect or fungal attack or are constitutively expressed in tissues vulnerable to pathogen attack [49–51]. The *Agave* chitinases are catalytically active and conserve the aromatic residues involved in the interaction with the substrate and also the catalytic residues Glu129 and Glu151 (Fig. 1A), including the His-Glu-Thr-Thr motif, which is highly conserved among class I chitinases [52]. The CBM18 also conserves the residues involved in interactions with GlcNAc oligosaccharides (Ser19, Phe21, Tyr23, and Tyr30) [28] (Fig. 1A). Analysis of the hydrolytic activity of both enzymes on colloidal chitin revealed an optimum pH of 5.0, and they were stable over a wide pH range (2.0–10.0), preserving over 75% of their enzymatic activities when incubated in different buffers for 48 h. These optimum pH and pH stability have been reported for other plant chitinases, including *Trichosanthes dioica* (pointed gourd), fruits from the genus *Diospyrus* (persimmon), leaf from *A. comosus* (pineapple), and *Ficus microcarpa* (Chinese banyan), and *Limonium bicolor* (lavender) [15,53,54]. However, not all plant chitinases show this pH stability, as has been demonstrated for those from *Carica papaya*, *Vicia faba* (fava bean), and *Vitis vinifera* (grapes), which were unstable in a broad pH range [55–57]. Furthermore, AtChi1 and AtChi2 showed high thermostabilities, as determined by thermal shift assays, with apparent T_m of 75 °C and 71 °C, respectively (Fig. 3C). Highly thermostable plant chitinases are not

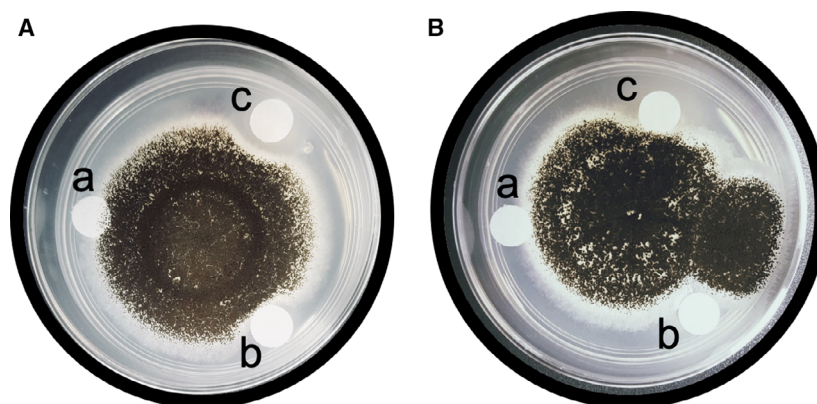


Fig. 7. Antifungal activities against the phytopathogenic fungus *Aspergillus* sp. (A) AtChi1; (B) AtChi2. (a) Left disks containing sterile buffer were used as negative controls. (b) Bottom disks containing 150 µg enzyme and (c) top disks containing 300 µg enzyme in a sterile 20 mm MES, pH 6.0 solution were applied onto potato dextrose agar in Petri dishes (5.4 cm diameter), each with a central inoculum that contained the mycelium of a 1-day-old fungi culture. Radial growth inhibition is clearly observed for both enzymes at the two concentrations used.

very common, regardless of the class or family to which they belong [54]. For instance, chitinases isolated from fava bean, cranberry beans, and maize were stable only at temperatures under 58 °C, 45 °C, and 60 °C, respectively [57–59]. However, there are some examples of chitinases that retained their activities above 60 °C, such as the chitinase isolated from persimmon, or up to 70 °C for the chitinases isolated from the ‘Baozhu’ pear and pineapple [3,15,54].

The kinetic analysis of AtChi1 and AtChi2 using colloidal chitin as the substrate (Fig. 3B), allowed us to obtain the K_m and V_{max} and to calculate k_{cat} and k_{cat}/K_m . The K_m values for these enzymes are about one order of magnitude lower than, or similar to, those reported for other plant chitinases when the same substrate was used. For instance, a class I chitinase from persimmon exhibited a K_m of $11.9 \pm 0.78 \text{ mg}\cdot\text{mL}^{-1}$ [54], and a class I/GH19 chitinase from *O. sativa* showed a K_m value $1.9 \text{ mg}\cdot\text{mL}^{-1}$ [60]. However, in these reports, the k_{cat} values are not shown. There is one report of a chitinase from the Cucurbitaceae *Trichosanthes dioica* which shows a K_m value of $0.3 \text{ mg}\cdot\text{mL}^{-1}$ and a V_{max} of $5.58 \text{ U}\cdot\text{min}^{-1}\cdot\text{mg}^{-1}$ [53]. These results are expected because the alignment of the Agave enzymes with class I plant chitinases showed good conservation of the catalytic residues and also of almost all the residues involved in substrate binding and catalysis [18,29,31].

To date, there are no reports of the three-dimensional structure of full-length class I chitinases. Some studies describe the structures of the CatD and the CBM18 separately; however, it has not been possible to obtain a good electron density map to interpret the long flexible linker connecting both [27,61,62]. Additionally, it has also been suggested that such linkers could be very labile [31]. In this regard, the only crystallographic structure of a class I chitinase lacks coordinates for the linker [18]. We performed SAXS experiments in solution to estimate the low-resolution molecular envelopes for both enzymes. The estimated radius of gyration (R_g) was 26.1 and 24.1 Å for AtChi1 and AtChi2, respectively. These values are in agreement with the 22.9 Å obtained for rice class I chitinase (OsChia1b) [18]. Furthermore, the experimental $P(r)$ curves for the enzymes exhibit asymmetric bell-shaped profiles, with a small additional maximum near to 78 and 58 Å for AtChi1 and AtChi2, respectively (Fig. 5B). This result suggests that both proteins are not globular particles with a spherically symmetric distribution of mass, and could have multiple conformations in solution, which is possible for multi-domain proteins connected by very long and flexible linkers [63]. These graphics allowed us to determine the maximum particle size (D_{max}), being

97.6 Å for AtChi1 and 98 Å for AtChi2. Both D_{max} values (Fig. 5B) are larger than the one obtained for OsChia1b (D_{max} of 86 Å) [18].

The low-resolution macromolecular shapes of both chitinases in solution showed slight differences in their overall shapes. Both models displayed elongated envelopes and had two lobes that were clearly distinguishable (Fig. 5C). However, the most important result revealed from these experiments is the clearly distinguishable presence of the long flexible linker that connects the CatD to the CBM18.

The theoretical 3D models of the two chitinases generated using the Robetta server were superimposed onto the *ab-initio* envelopes calculated using the SAXS data (Fig. 5C). In general, the conformation of both models is in good agreement with the SAXS envelopes, with slight discrepancies mainly due to the flexibility of the linker. The template used by Robetta to generate the CBMs models was the crystal structure of rice class I chitinase (PDB entry 2DKV), which lacks coordinates for the linker. This structure was selected due to high sequence identity, 68% for AtChi1 and 67% for AtChi2. To build the catalytic domains, the crystal structure of the rye chitinase (PDB entry 4DWX) was used by Robetta due to sequence identity (76.5%). It is important to mention that Robetta does not consider the flexibility of the linker. These models showed 99.1% and 99.5% of the residues in the most favored region of the Ramachandran plot, respectively, and only 0.9% and 0.5% in the disallowed regions, respectively [36]. The residues in the disallowed regions of the Ramachandran plot, two in AtChi1 and one in AtChi2 are located in the chitin binding groove, indicating commonly strained conformations of residues in binding sites [37]. Interestingly, our models suggest a slightly higher spatial proximity of the CBM18 with the CatD for AtChi2 (Fig. 5D). Recently, the NMR structure of the chitinase CJP-4 from the Japanese cedar pollen showed that the CBM18 was responsible for chitin binding [31]; therefore, the separation found between the CBM18s and the CatDs in a hypothetical open conformation could contribute to the decrease in the catalytic efficiency of these enzymes, as was observed for AtChi2 in comparison with AtChi1. The shapes of the envelopes obtained in our work suggest the presence of at least two conformations in solution for this class of enzymes. Considering that most of the different residues between AtChi1 and AtChi2 are close to the interface between the two domains and on the opposite side of the catalytic groove (Fig. 5A,C), we suggest that these residues may participate in the stabilization of the open or the compact conformation during the catalysis of class I chitinases and may

contribute to the abundance of each conformation and its functional differences. This hypothesis is supported with the results from the ITC experiments (Fig. 4), where the thermodynamics of binding for the chitohexaose substrate were measured under conditions promoting low catalytic activity. The results show relevant differences between the two chitinases. First, the binding of chitohexaose is enthalpically driven for both enzymes; however, AtChi2 displays an entropic penalty 10-fold lower than the one for AtChi1. Nonetheless, there is no significant difference in the binding free energy ΔG , suggesting that all six GlcNAc moieties of the chitohexaose associate to the binding cleft in the two chitinases [64]. Furthermore, the oligosaccharide binds twofold more tightly to AtChi2 with a K_d of 128 μM , whereas AtChi1 displays a K_d of 208 μM . These values are well in agreement with a previous report for a class IV chitinase from *Cryptomeria japonica* [31]. Taken together, these data suggest that the six different residues between the two chitinases have long-range effects in the accommodation process of the ligand in the binding groove and affect its affinity even when they are located on the surface of the two proteins. Differences in the thermodynamic parameters indicate that subtle changes in the amino acid sequence of the chitinases promote divergence in the formation of the protein–ligand complex.

The docking experiments suggest that the active site groove is different in both isoforms with more flexibility of the oligosaccharide in the binding groove of AtChi2 (Fig. S4). Figure 6A indicates that loop III in AtChi1 is conformationally different from the same loop in AtChi2. This causes that the catalytic residue Glu151 is farther from the ligand in AtChi2. These results could explain the differences in K_m and K_d values between both enzymes. The calculated docking binding energies are in good agreement with the experimental values obtained in the ITC. Therefore, we consider that our simulations are valid.

Besides, Fig. 5C shows all the residues in the groove of AtChi1 and AtChi2 that make contact with the oligosaccharide, just a few residues are not conserved in these interactions. Several residues (shown in transparent) located in loops II and V, adopt different conformation probably due to the six different residues in both enzymes. Long-distance effects of these mutations could be also responsible for small changes in the binding sites of the enzymes. Notably, in both enzymes, the position of the catalytic Glu151 is far from the $-1 +1$ GlnNAc bond in the chitohexaose molecule, which could explain the low catalytic activity over oligosaccharides. The distances between the OE1-Glu151 to the $-1 +1$ GlnNAc bond is 5.56 Å (AtChi1)

and 5.81 Å (AtChi2); and for OE1-Glu129 the distances are 7.50 Å for AtChi1 and 5.30 Å for AtChi2 (Fig. 6B). Besides, we measured the distance between the C α of the catalytic proton donor and the catalytic nucleophile in each enzyme and the values are 9.48 and 9.31 Å, indicating that they operate through an inverting mechanism of action.

Interestingly, AtChi1 and AtChi2 showed antifungal activities versus *Aspergillus* sp. at concentrations of 150 and 300 μg per disk. This result suggests that the *Agave* enzymes are involved in defense mechanisms. The inhibition observed was lower than that reported for other plant chitinases [3,54]; however, it is known that plants overexpress a pull of chitinases, glucanases, and others PR proteins that act synergistically to fight pathogen infections [65]. These inhibitory concentration values are similar to those reported for barley class I chitinase of 80 and 200 μg [66]. Recently, the variation in the temporal and spatial induction of chitinases in response to infection was demonstrated in chickpea [47]. Therefore, in the late stages of the infection, chitinases that maintain their expression may have additional physiological functions in the plant, not directly related to defense.

Our results are the first into the study of chitinases enzymes of *A. tequilana* and in the whole genus *Agave*. The information provided by the experimental SAXS analysis showed the spatial organization of the two domains, characteristic of class I chitinases. The different residues located near the inter-domain region could be responsible for the slightly different conformations of both chitinases, the differences in the kinetic properties and also the different thermodynamic parameters, which could promote divergence in the formation of the protein–ligand complex. In this regard, it has been recognized that mutations can exert long-distance effects on protein structure, flexibility and stability [67]. Finally, we also demonstrated that both enzymes, one of which (AtChi2) was obtained from RNA of *F. oxysporum*-infected plants, exhibit antifungal activity versus *Aspergillus* sp.; therefore, these enzymes could be considered as pathogenesis-related proteins (PR) with an important role in *Agave* defense.

Materials and methods

Materials

Escherichia coli DH10 α and Rosetta Gami strains were from Novagen (Madison, WI, USA) and SHuffle c3029 strain was purchased from New England BioLabs (Ipswich, MA, USA). The pJET1.2/blunt vector was from Thermofisher (Waltham, MA, USA). The plasmids

pET-32a and pMCSG7 were from Novagen and SnapGene (IA, USA), respectively. Plants of *A. tequilana* used in RNA isolation were collected in an Agave plantation in Atotonilco el Alto Jalisco, Mexico. These plants were cultivated on autoclaved soil and maintained at 23 °C.

Identification of a predicted chitinase

The gene sequence of a class I chitinase was searched on the *A. tequilana* transcriptome (BioProject PRJNA193469) [68] using conserved regions of different plant chitinases with antifungal properties. The whole gene was assembled and submitted for a nucleotide BLAST alignment using the NCBI server [24]. The assembled sequence lacking the signal peptide was synthesized by GenScrip (Piscataway, NJ, USA) and cloned into the pET-32a vector with a TEV protease site, instead of the EK site, to produce the recombinant protein, which was named AtChi1. The TEV protease is produced 'in-house' [69].

Cloning of the chitinase gene (AtChi2)

To verify the presence of the hypothetical chitinase (AtChi1) in the genome of *A. tequilana*, RNA was extracted from leaves, roots, and stems of healthy and *F. oxysporum* infected *A. tequilana* plants. *F. oxysporum* inoculum was produced in sterile rice grains and was mixed with the soil where the *A. tequilana* plant would be transplanted. After 45 days, 50 000 propagules of *F. oxysporum* were obtained per gram of soil and the *A. tequilana* plant was transplanted and left to grow for 4 and 7 weeks. The plant material was washed with DEPC-treated water, cut into small pieces, frozen in liquid nitrogen and macerated using a mortar and then was treated with TRizol (Sigma, St. Louis, MO, USA) according to the manufacturer's instructions. Briefly, 1 mL of TRizol was added to 100 mg of macerated tissue, incubated at 22 °C during 30 min and then centrifuged to eliminate large debris, 200 µL of chloroform was added to the clear supernatant, incubated 10 min at room temperature and then centrifuged for 15 min at 12 000 *g* at 4 °C. RNA was precipitated by adding 0.5 mL of isopropanol to the aqueous phase; the RNA pellet was then washed with 75% ethanol and resuspended with 50 µL RNAase-free water. RNA yield was calculated by absorbance at 260 nm and sample purity was determined by absorbance at 280 nm and RNA agarose gel electrophoresis. A calculated A_{260}/A_{280} ratio of the sample was 1.99.

Once the RNA was isolated, cDNA was synthesized using the ProtoScript® II First Strand cDNA Synthesis Kit (New England BioLabs), 500 µg of total RNA were used in a first strand cDNA synthesis reaction with 50 units of ProtoScript II Reverse Transcriptase and 5 µM of oligo d(t)23VN. Reactions were incubated at 42 °C for 1 h, then 5 min at 80 °C to inactivate the enzyme and then diluted with nuclease-free water to a final volume of 50 µL. The PCR was performed

using KAPA HiFi DNA polymerase in a 50 µL total volume containing, KAPA HiFi HotStart ReadyMix 1X (KapaBiosystems Inc, Wilmington, MA, USA), 0.3 µM of each primer, and 2–5 µL of cDNA. The primer sequences were: 5'-GCTCCCACGCACAGCAATGTGGGAGCC-3' (forward) and 5'-CTAAAAATGACTCTGGTTCCCA CAGTCC-3' (reverse). The PCR was carried out on a Techne cycler under the following conditions: an initial denaturation step at 95 °C for 3 min, followed by 30 cycles at 98 °C for 20 s, 65 °C for 30 s, 72 °C for 2 min, with a final extension at 72 °C for 5 min. PCR products were analyzed by 1% agarose gel stained with ethidium bromide. No amplification of the gene was observed in either sample of the healthy Agave; however, the amplification of the gene was observed in leaves of infected plants.

The gene was cloned into the pJET1.2/blunt vector (Thermo Scientific CloneJET PCR Cloning Kit). The cloning reaction was set to a final volume of 20 µL using 10 µL of 2× reaction buffer, 2 µL of non-purified PCR product, 50 ng of pJET1.2/blunt cloning vector, and 1 µL of T4 ligase; incubation was done at 22 °C for 30 min and 5 µL of the ligation mixture were used for heat-shock transformation of *E. coli* DH5α-competent cells. The positive clones were confirmed by sequencing and after the analysis of the sequences cloned, six differences between the hypothetical protein from bio project and the protein cloned from RNA were found; for this reason, the last one was named AtChi2.

To obtain the recombinant AtChi2 protein, subcloning the gene into the pET-32a vector under the same conditions as AtChi1 was tried. A new pair of primers were designed adding a *KpnI* and TEV sites into the forward primer, and an *EcoRI* restriction site into the reverse primer, unfortunately no positive clone was obtained after several attempts. The expression plasmid for recombinant AtChi2 was constructed via ligation-independent cloning [70]. The pMCSG7 was linearized with *SspI* restriction enzyme. The AtChi1 gene cloned into pJET1.2 vector was amplified with forward primer 5'-TACTTCCAATCCAATGCGCAG CAATGTGGGAGCC-3' and reverse primer 5'-TTATC CACTTCCAATGCTAAAAATGACTCTGGTTCCCA CA GTCC-3'. The single-stranded cohesive ends of the PCR product and linear vector were produced via the treatment of T4 DNA polymerase in the presence of only dCTP or dGTP, respectively, to generate complementary overhangs. The two treated segments were mixed and allowed to anneal without ligase. The vector, designated as pMCSG7-AtChi2, was then heat-shock transformed into *E. coli* DH5α, and positive clones of the recombinant plasmid were identified, propagated and sequenced.

Heterologous expression and purification of AtChi1 and AtChi2

To express AtChi1, the Rosetta gami strain was cultivated in Luria-Bertani media at 37 °C with agitation until an

A_{600} of 0.5 was reached. IPTG was added to a final concentration of 0.5 mM and the incubation temperature lowered to 18 °C for 16 h. Likewise, the SHuffle strain containing AtChi2 was cultivated at 30 °C until an A_{600} of 0.7 was reached. Induction was achieved with the addition of 1 mM IPTG at 16 °C for 18 h. In both cases, the cells were harvested by centrifugation at 15 300 *g* and suspended in the lysis buffer containing 20 mM Tris/HCl, pH 8.0; 300 mM NaCl; 1 mM PMSF. Cell pellets were lysed by sonication and clarified by centrifuging at 30 000 *g* for 45 min.

The purification protocol was the same for both AtChi1 and AtChi2 proteins. The supernatants were loaded onto HisTrap columns (GE Healthcare, Piscataway, NJ, USA) equilibrated using five column volumes of 20 mM Tris/HCl, pH 8.0, 300 mM NaCl, 20 mM imidazole; the columns were washed with equilibration buffer and the proteins eluted using an imidazole concentration gradient (60% of the elution buffer containing 20 mM Tris/HCl, pH 8.0, 0.4 M imidazole). The purified fusion proteins were cleaved overnight at 4 °C, with agitation with TEV protease (50 mM Tris-HCl, pH 8.0, 300 mM NaCl, 5 mM MgCl₂ 0.25 mM DTT, and 5% glycerol) and the products were recirculated through the HisTrap column. The unbound fractions were then concentrated and applied to a Superdex 75 16/60 size exclusion column. To assess each purification step, SDS/PAGE and Coomassie blue staining were used [71]. Protein concentration was determined using the theoretical extinction coefficients of 1 mg·mL⁻¹ solutions of AtChi1 and AtChi2 at 280 nm, of 1.76 and 1.71, respectively. Finally, monodispersity and oligomerization of the samples were verified using a Malvern Zetasizer μ V instrument (Malvern Panalytical Ltd, Malvern, UK).

Mass, pI determination, and circular dichroism measurements

To determine the molecular mass of the recombinant proteins, matrix-assisted laser desorption/ionization-time of flight (MALDI-TOF) mass spectrometry was used (Microflex; Bruker Scientific LLC, Billerica, MA, USA), 20 μ g of each protein was used for the analysis. The standard for mass calibration was rabbit triosephosphate isomerase (M_r 32.62 kDa). The matrix used was a saturated solution of sinapinic acid in 30% (v/v) aqueous acetonitrile, 0.1% (v/v) trifluoroacetic acid. Samples were analyzed using FLEX ANALYSIS 3.0™ (Bruker) software. Isoelectric points were determined using a PhastSystem and PhastGel IEF in the pH range 3–9 (GE Healthcare Life Sciences).

CD measurements were performed at 20 °C using a Jasco-J1500 spectropolarimeter (Jasco, Easton, MD, USA) equipped with a Peltier temperature control system. Solutions of AtChi1 and AtChi2, at a concentration of 0.2 mg·mL⁻¹, were dialyzed against deionized water using Spectra/Por dialysis membrane (MWCO 6000–8000) and filtered with Durapore membrane filters (0.22 μ m pore size). Far-UV spectra

were collected for each sample from 185 to 260 nm in a 1-mm path-length cell. Three scans were averaged to obtain the final spectra of the two proteins. All the spectra were scaled to molar ellipticities $[\theta]$ (deg·cm²·dmol⁻¹). The BeStSel (Beta Structure Selection) server was used to analyze the CD spectra of both enzymes [72].

Determination of the optimum pH and pH stability with colloidal chitin

The optimum pH for each chitinase was determined at 37 °C using different buffers at 20 mM concentration and pH values between 3.0 and 10.0. The buffers used were monobasic sodium phosphate/phosphoric acid, sodium acetate (pH 3.0); sodium acetate/acetic acid (pH 4.0 and 5.0); dibasic potassium phosphate/phosphoric acid (pH 6.0 and 7.0); and Tris base/hydrochloric acid (pH 8.0–10.0). To check pH stability, the enzyme was incubated in the above-mentioned buffers at 4 °C for 48 h. After incubation, samples were added into the reaction mixture and the residual activities were measured at the optimum pH (5.0).

Thermal shift assays

The thermodynamic stabilities of the chitinases were determined using fluorescence-based thermal shift assays with kits to screen pH, stability, and solubility using the environmentally sensitive extrinsic dye SYPRO Orange [73]. Assays were performed in 96-well plates using 20 μ L of chitinases that contained SYPRO Orange dye and were recorded with a Q-PCR instrument, while the temperature was increased in a continuous step from 25 to 95 °C.

Chitinase assays and substrate specificity

The chitinase activity assays were performed using colloidal chitin, chitohexaose, and chitotriose as substrates and products were quantified with the 3,5-dinitrosalicylic acid (DNS) method that detects reducing sugars [74,75]. For the steady-state kinetics with colloidal chitin, 1.4 mL final volume reactions were set at 16 different substrate concentrations between 0.12 and 19.4 mg·mL⁻¹, all reactions started with the addition of 200 μ g of enzyme in 50 mM acetate buffer, pH 5.0 at 37 °C with gentle shaking for 24 h, after which the tubes of reaction were centrifuged at 14 000 *g* for 5 min. Then, 0.7 mL of the DNS reagent was added to 0.4 mL of the supernatant and the mixture was boiled for 15 min. After cooling at room temperature, the absorbance at 550 nm was measured. A standard curve was prepared using *N*-Acetyl-D-Glucosamine. One enzyme unit was defined as the quantity of enzyme necessary to release 1 nmol of *N*-Acetyl-D-Glucosamine from colloidal chitin in 1 h under the assay conditions. All measurements were performed in triplicate, with negative controls comprising

mixes without enzyme. The results were adjusted using a Michaelis–Menten equation in the GRAPHPAD software (San Diego, CA, USA) to obtain the K_m and V_{max} values.

For substrate specificity using chitotriose and chito-hexaose the same methodology described for colloidal chitin was used. Besides, to determine chitobiosidase and exochitinase activities, a fluorometric assay with 4-Methylumbelliferyl *N*-acetyl- β -D-glucosaminide and 4-Methylumbelliferyl- β -D-*N,N'*-diacetylchitobioside (Sigma, St. Louis, MO, USA) was used. The amount of 4-methylumbelliferone (4-MU) released was measured spectrofluorometrically by a fluorescence spectrophotometer (Biotek Synergy HT, Biotek Instruments, Winooski, VT, USA) (excitation 390 nm and emission 450 nm). Each of the substrates was dissolved in 0.5 mL of 50 mM sodium acetate buffer (pH 5.0) to give 0.036 mM substrate solutions. Ten microlitre of the enzyme solution (1.48 mg·mL⁻¹) was added to the substrate solution and the mixture was incubated at 37 °C. As a control, the substrate solution was also incubated in the absence of chitinase. A portion (0.1 mL) of the reaction mixture was withdrawn after an appropriate reaction time and mixed with 0.5 mL of 0.4 M Na₂HPO₄–NaOH buffer, pH 11.9, to terminate the enzymatic reaction. The fluorescence intensity of the resultant solution was measured at 450 nm with excitation at 360 nm using a Shimadzu RF1500 spectrofluorometer (Shimadzu Corp., Kyoto, Japan). The concentration of 4-MU released from the fluorogenic substrates was calculated from a calibration curve obtained using authentic solutions of UMB after subtraction of the control value.

Isothermal titration calorimetry assays

ChiAt1 and ChiAt2 were exhaustively dialyzed against 20 mM phosphate buffer pH 7.0 and concentrated, using Amicon-Ultra 0.5 (Millipore Sigma, St. Louis, MO, USA; MWCO 10 kDa) centrifugal filter units, to a final concentration of 100 μ M. Chitohexaose was dissolved in the dialysis buffer to obtain a 6.7 mM solution. ITC measurements for both chitinases with chitohexaose were performed at 290 K using a low-volume (200 μ L sample cell) NanoITC200 (Microcal, Malvern Panalytical Ltd). The pH value and temperature were selected to measure essentially binding and not hydrolysis of chitohexaose. The binding reaction was monitored by recording the heat release upon small additions of the chito-hexaose solution to each protein solution. In the experiment, 33 injections (1.2 μ L each) of the chito-hexaose solution were titrated into the protein solution. The solution was stirred at 350 r.p.m. and the resulting heat of reaction was measured. The heat of dilution of the chito-hexaose was obtained by titrating the ligand into the buffer solution, under identical conditions and injection schedule used with the enzyme samples. The enthalpy change (ΔH) and binding constant (K_d) were determined from the experimental curve using the software ORIGIN version 7.0.

Small angle x-ray scattering analysis

Scattering data were collected at the Experimental Station 4-2 (Stanford Synchrotron Radiation Lightsource). For AtChi1, the detector used was a Rayonix MX225HE CCD and for AtChi2 a Pilatus3 X 1M detector (Dectris, Philadelphia, PA, USA). The measurements were made using protein concentrations of 0.23, to 15 mg·mL⁻¹, in 50 mM MES buffer, pH 6, at 15 °C. This buffer was selected for SAXS experiments because thermal shift assays gave the highest stability of both enzymes in these conditions (Fig. 3C). For data analysis of AtChi1, we used the lowest protein concentration because some aggregation was observed during the experiment. It is important to note that before the experiment, the protein was in a monodisperse and monomeric form, as determined with the DLS instrument. For AtChi2, we used a merged file with the 7.5 and 3.75 mg·mL⁻¹ concentrations for the analysis. The wavelength of the x-rays was 1.127 Å and the sample-detector distance 1.7 m, which gave a measured range of $0.007 < q < 0.5 \text{ \AA}^{-1}$ ($q = 4\pi\sin\theta/\lambda$, where 2θ is the scattering angle and λ is the wavelength). Background scattering was subtracted, and data were analyzed using the ATSAS software package [76]. The radius of gyration (R_g) for each protein was calculated using the Guinier approximation with the program PRIMUS [77]. The pair distribution function $P(r)$, and the maximum particle size (D_{max}) were obtained using the program GNOM [78]. To generate *ab-initio* envelopes, ten cycles of DAMMIF [33] were run and were followed by the program DAMFIL [34] to obtain low-resolution envelopes. The UCSF CHIMERA package was used to fit models generated using Robetta (<http://robeta.bakerlab.org>) for both chitinases into the SAXS envelopes and to prepare figures [79]. The CRYSOLOG program [38] was used for calculating the fitting of each model to SAXS data before and after the minimization.

Docking simulation

We performed *in silico* molecular-docking simulations of the (GlcNAc)₆ oligosaccharide with AUTODOCK 4.0 [80] using the models generated in Robetta of the CatDs of both Agave chitinases. Prior to docking, the chito-hexaose coordinates were generated with SMILES and minimized in CHIMERA [79]. The monosaccharides in (GlcNAc)₆ were named as -4, -3, -2, -1 and +1, +2, beginning from the non-reducing end. Hydrogens and charges were assigned to the receptor and the ligands using the AUTODOCKTOOLS 1.5.7 [80]. Docking simulations were run using the Lamarckian Genetic algorithm that is known to be the most efficient and reliable method of Auto Dock. The grid maps were calculated using AutoGrid. Initially, potential binding sites were detected based on a blind docking in which the box was sufficiently large to cover the CatDs centered at their midpoints (48.75 Å × 43.5 Å × 38.6 Å) along the *x*-, *y*-

and z-axes. The next step was a focused docking with a smaller box (26.3 Å × 22.5 Å × 22.5 Å), centered on the carbohydrate-binding groove of the CatD that was the best energy result obtained in the blind docking. The best models were selected based on binding energy scores. We identified and analyzed the residues potentially involved in ligand binding using CHIMERA [79].

Antifungal activity assays

Antifungal activity of AtCh1 and AtChi2 was conducted using the disk diffusion test. The inhibitory effect of the chitinases was tested on the radial growth of the phytopathogenic fungus of economic importance *Aspergillus* sp. Two different amounts of the purified chitinases, 150 and 300 µg in a sterile 20 mM MES, pH 6.0 solution, were applied to 5-mm sterile paper disks onto potato dextrose agar in Petri dishes (5.4 cm diameter), each with a central inoculum that contained the mycelium of a 1-day-old fungi culture. The disks were placed on the agar 24 h after the inoculation at an approximate distance of 5 mm from the growing front of the hyphae. The plates were incubated for 48 h at 22 °C and analyzed. Disks with sterile buffer were used as negative controls.

Acknowledgements

We thank Jose Rivera from the IQ-UNAM for kindly performing the antifungal experiments and Javier Plasencia from FQ-UNAM for donating the *F. oxysporum* strain. We also thank Alfredo Torres Larios from IFC-UNAM for allowing us to use some resources of his laboratory. We thank T. Matsui and T. Weiss for technical support in SAXS data collection using the Stanford Synchrotron Radiation Lightsource. SLAC National Accelerator Laboratory is supported by the U.S. Department of Energy, Office of Science, Office of Basic Energy Sciences under Contract No. DE-AC02-76SF00515. The SSRL Structural Molecular Biology Program is supported by the DOE Office of Biological and Environmental Research, and by the National Institutes of Health, National Institute of General Medical Sciences (including P41GM103393). We also thank LANEM-IQ-UNAM for technical support in crystals characterization. The contents of this publication are solely the responsibility of the authors and do not necessarily represent the official views of NIGMS or NIH. This work was supported by CONACyT (Grant 221169 to AR-R) and DGAPA-PAPIIT (IN208418 to AR-R). Yusvel Sierra Gómez is a doctoral student from the Programa de Doctorado en Ciencias Biomédicas, Universidad Nacional Autónoma de México (UNAM) who received fellowship 512410 from CONACyT.

Author contributions

YS-G: Planned and performed experiments, analyzed the data, and co-wrote the manuscript; AR-H: performed experiments, analyzed data, and revised the document; PC-S: planned and performed experiments; HG-V: performed ITC experiments; AH-S: performed experiments and analyzed the data; DS: processed and analyzed the SAXS data; AR-R: conceived the idea, planned experiments, analyzed the data, and co-wrote the manuscript.

Conflict of interest

The authors declare no conflict of interest.

References

- 1 Hamid R, Khan MA, Ahmad M, Ahmad MM, Abidin MZ, Musarrat J & Javed S (2013) Chitinases: an update. *J Pharm Bioallied Sci* **5**, 24–29.
- 2 Goni O, Sanchez-Ballesta MT, Merodio C & Escribano MI (2013) Two cold-induced family 19 glycosyl hydrolases from cherimoya (*Annona cherimola*) fruit: an antifungal chitinase and a cold-adapted chitinase. *Phytochemistry* **95**, 94–104.
- 3 Han P, Yang CC, Liang XB & Li LR (2016) Identification and characterization of a novel chitinase with antifungal activity from ‘Baozhu’ pear (*Pyrus ussuriensis* Maxim.). *Food Chem* **196**, 808–814.
- 4 Taira T, Ohnuma T, Yamagami T, Aso Y, Ishiguro M & Ishihara M (2002) Antifungal activity of rye (*Secale cereale*) seed chitinases: the different binding manner of class I and class II chitinases to the fungal cell walls. *Biosci Biotechnol Biochem* **66**, 970–977.
- 5 Iseli B, Armand S, Boller T, Neuhaus JM & Henrissat B (1996) Plant chitinases use two different hydrolytic mechanisms. *FEBS Lett* **382**, 186–188.
- 6 Oyeleye A & Normi YM (2018) Chitinase: diversity, limitations, and trends in engineering for suitable applications. *Biosci Rep* **38**. <https://doi.org/10.1042/BSR20180323>
- 7 Beintema JJ (1994) Structural features of plant chitinases and chitin-binding proteins. *FEBS Lett* **350**, 159–163.
- 8 Kasprzewska A (2003) Plant chitinases – regulation and function. *Cell Mol Biol Lett* **8**, 809–824.
- 9 Neuhaus JM, Fritig B, Linthorst HJM, Meins F, Mikkelsen JD & Ryals J (1996) A revised nomenclature for chitinase genes. *Plant Mol Biol Rep* **14**, 102–104.
- 10 Su YC, Xu LP, Wang SS, Wang ZQ, Yang YT, Chen Y & Que YX (2015) Identification, phylogeny, and transcript of chitinase family genes in sugarcane. *Sci Rep* **5**, 10708.

- 11 van Loon LC, Rep M & Pieterse CMJ (2006) Significance of inducible defense-related proteins in infected plants. *Annu Rev Phytopathol* **44**, 135–162.
- 12 Legrand M, Kauffmann S, Geoffroy P & Fritig B (1987) Biological function of pathogenesis-related proteins: four tobacco pathogenesis-related proteins are chitinases. *Proc Natl Acad Sci USA* **84**, 6750–6754.
- 13 Hawkins LK, Mylroie JE, Oliveira DA, Smith JS, Ozkan S, Windham GL, Williams WP & Warburton ML (2015) Characterization of the maize chitinase genes and their effect on *Aspergillus flavus* and aflatoxin accumulation resistance. *PLoS One* **10**, e0126185.
- 14 Krishnaveni S, Liang GH, Muthukrishnan S & Manickam A (1999) Purification and partial characterization of chitinases from sorghum seeds. *Plant Sci* **144**, 1–7.
- 15 Taira T, Toma N & Ishihara M (2005) Purification, characterization, and antifungal activity of chitinases from pineapple (*Ananas comosus*) leaf. *Biosci Biotechnol Biochem* **69**, 189–196.
- 16 Huet J, Rucktooa P, Clantin B, Azarkan M, Looze Y, Villeret V & Wintjens R (2008) X-ray structure of papaya chitinase reveals the substrate binding mode of glycosyl hydrolase family 19 chitinases. *Biochemistry* **47**, 8283–8291.
- 17 Ohnuma T, Umemoto N, Kondo K, Numata T & Fukamizo T (2013) Complete subsite mapping of a “loopful” GH19 chitinase from rye seeds based on its crystal structure. *FEBS Lett* **587**, 2691–2697.
- 18 Kezuka Y, Kojima M, Mizuno R, Suzuki K, Watanabe T & Nonaka T (2010) Structure of full-length class I chitinase from rice revealed by X-ray crystallography and small-angle X-ray scattering. *Proteins* **78**, 2295–2305.
- 19 Sandhu JS, Sidhu MK & Yadav IS (2013) Control of fungal disease in agricultural crops by chitinase and glucanase transgenes. In *Sustainable Agriculture Reviews* (LichtfouseEE, ed.), pp. 163–194. Springer, Dordrecht.
- 20 Cortes-Romero C, Martinez-Hernandez A, Mellado-Mojica E, Lopez MG & Simpson J (2012) Molecular and functional characterization of novel fructosyltransferases and invertases from *Agave tequilana*. *PLoS One* **7**, e35878.
- 21 Davis SC, Dohleman FG & Long SP (2011) The global potential for Agave as a biofuel feedstock. *GCB Bioenergy* **3**, 68–78.
- 22 Farias-Sanchez JC, Velazquez-Valadez U, Vargas-Santillan A, Pineda-Pimentel MG, Mendoza-Chavez EA, Rutiaga-Quinones JG, Saucedo-Luna J & Castro-Montoya AJ (2016) Production of fermentable sugars and hydrogen-rich gas from *Agave tequilana* biomass. *Bioenergy Res* **9**, 1015–1022.
- 23 Vargas-Maya NI, Gonzalez-Hernandez GA, Padilla-Guerrero IE & Torres-Guzman JC (2017) Overexpression of smORF YNR034W-A/EGO4 in *Saccharomyces cerevisiae* increases the fermentative efficiency of *Agave tequilana* Weber must. *J Ind Microbiol Biotechnol* **44**, 63–74.
- 24 Altschul SF, Madden TL, Schaffer AA, Zhang JH, Zhang Z, Miller W & Lipman DJ (1997) Gapped BLAST and PSI-BLAST: a new generation of protein database search programs. *Nucleic Acids Res* **25**, 3389–3402.
- 25 Petersen TN, Brunak S, von Heijne G & Nielsen H (2011) SignalP 4.0: discriminating signal peptides from transmembrane regions. *Nat Methods* **8**, 785–786.
- 26 Kall L, Krogh A & Sonnhammer ELL (2007) Advantages of combined transmembrane topology and signal peptide prediction – the Phobias web server. *Nucleic Acids Res* **35**, W429–W432.
- 27 Martinez-Caballero S, Cano-Sanchez P, Mares-Mejia I, Diaz-Sanchez AG, Macias-Rubalcava ML, Hermoso JA & Rodriguez-Romero A (2014) Comparative study of two GH19 chitinase-like proteins from *Hevea brasiliensis*, one exhibiting a novel carbohydrate-binding domain. *FEBS J* **281**, 4535–4554.
- 28 Reyes-Lopez CA, Hernandez-Santoyo A, Pedraza-Escalona M, Mendoza G, Hernandez-Arana A & Rodriguez-Romero A (2004) Insights into a conformational epitope of Hev b 6.02 (hevein). *Biochem Biophys Res Commun* **314**, 123–130.
- 29 Ohnuma T, Umemoto N, Nagata T, Shinya S, Numata T, Taira T & Fukamizo T (2014) Crystal structure of a “loopless” GH19 chitinase in complex with chitin tetrasaccharide spanning the catalytic center. *Biochim Biophys Acta* **1844**, 793–802.
- 30 Ohnuma T, Sorlie M, Fukuda T, Kawamoto N, Taira T & Fukamizo T (2011) Chitin oligosaccharide binding to a family GH19 chitinase from the moss *Bryum coronatum*. *FEBS J* **278**, 3991–4001.
- 31 Takashima T, Ohnuma T & Fukamizo T (2018) NMR analysis of substrate binding to a two-domain chitinase: comparison between soluble and insoluble chitins. *Carbohydr Res* **458**, 52–59.
- 32 Valentini E, Kikhney AG, Previtali G, Jeffries CM & Svergun DI (2015) SASBDB, a repository for biological small-angle scattering data. *Nucleic Acids Res* **43**, D357–D363.
- 33 Franke D & Svergun DI (2009) DAMMIF, a program for rapid ab-initio shape determination in small-angle scattering. *J Appl Crystallogr* **42**, 342–346.
- 34 Volkov VV & Svergun DI (2003) Uniqueness of ab initio shape determination in small-angle scattering. *J Appl Crystallogr* **36**, 860–864.
- 35 Kim DE, Chivian D & Baker D (2004) Protein structure prediction and analysis using the Robetta server. *Nucleic Acids Res* **32**, W526–W531.
- 36 Laskowski RA, MacArthur MW, Moss DS & Thornton JM (1993) Procheck – a program to check the

- stereochemical quality of protein structures. *J Appl Crystallogr* **26**, 283–291.
- 37 Herzberg O & Moult J (1991) Analysis of the steric strain in the polypeptide backbone of protein molecules. *Proteins* **11**, 223–229.
- 38 Svergun D, Barberato C & Koch MHJ (1995) CRYSOLE – a program to evaluate x-ray solution scattering of biological macromolecules from atomic coordinates. *J Appl Crystallogr* **28**, 768–773.
- 39 Winn MD, Ballard CC, Cowtan KD, Dodson EJ, Emsley P, Evans PR, Keegan RM, Krissinel EB, Leslie AGW, McCoy A *et al.* (2011) Overview of the CCP4 suite and current developments. *Acta Crystallogr D* **67**, 235–242.
- 40 Khan A, Nasir IA, Tabassum B, Aaliya K, Tariq M & Rao AQ (2017) Expression studies of chitinase gene in transgenic potato against *Alternaria solani*. *Plant Cell Tissue Organ Cult* **128**, 563–576.
- 41 Osman GH, Assem SK, Alreedy RM, El-Ghareeb DK, Basry MA, Rastogi A & Kalaji HM (2015) Development of insect resistant maize plants expressing a chitinase gene from the cotton leaf worm, *Spodoptera littoralis*. *Sci Rep* **5**, 18067.
- 42 Lee CG, Da Silva CA, Dela Cruz CS, Ahangari F, Ma B, Kang MJ, He CH, Takyar S & Elias JA (2011) Role of chitin and chitinase/chitinase-like proteins in inflammation, tissue remodeling, and injury. *Annu Rev Physiol* **73**, 479–501.
- 43 Vastrad B, Vastrad C, Godavarthi A & Chandrashekar R (2017) Molecular mechanisms underlying gliomas and glioblastoma pathogenesis revealed by bioinformatics analysis of microarray data. *Med Oncol* **34**, 182.
- 44 Xu T, Zhong CK, Wang AL, Guo ZR, Bu XQ, Zhou YP, Tian YF, HuangFu XF, Zhu ZB & Zhang YH (2017) YKL-40 is a novel biomarker for predicting hypertension incidence among prehypertensive subjects: A population-based nested case-control study in China. *Clin Chim Acta* **472**, 146–150.
- 45 Dahiya N, Tewari R & Hoondal GS (2006) Biotechnological aspects of chitinolytic enzymes: a review. *Appl Microbiol Biotechnol* **71**, 773–782.
- 46 Kowsari M, Motallebi M & Zamani M (2014) Protein engineering of Chit42 towards improvement of chitinase and antifungal activities. *Curr Microbiol* **68**, 495–502.
- 47 Datta J & Lal N (2018) Induced temporal and spatial variation in host defence enzymes in response to *Fusarium* wilt in Chickpea. *J Microbiol Biotechnol Food Sci* **7**, 426–431.
- 48 Bishop JG, Dean AM & Mitchell-Olds T (2000) Rapid evolution in plant chitinases: molecular targets of selection in plant-pathogen coevolution. *Proc Natl Acad Sci USA* **97**, 5322–5327.
- 49 Backiyarani S, Uma S, Nithya S, Chandrasekar A, Saraswathi MS, Thangavelu R, Mayilvaganan M, Sundararaju P & Singh NK (2015) Genome-wide analysis and differential expression of chitinases in banana against root lesion nematode (*Pratylenchus coffeae*) and eumusa leaf spot (*Mycosphaerella eumusae*) pathogens. *Appl Biochem Biotechnol* **175**, 3585–3598.
- 50 Bagnaresi P, Biselli C, Orru L, Urso S, Crispino L, Abbruscato P, Piffanelli P, Lupotto E, Cattivelli L & Vale G (2012) Comparative transcriptome profiling of the early response to *Magnaporthe oryzae* in durable resistant vs susceptible rice (*Oryza sativa* L.) genotypes. *PLoS One* **7**, e51609.
- 51 Samac DA, Hironaka CM, Yallaly PE & Shah DM (1990) Isolation and characterization of the genes encoding basic and acidic chitinase in *Arabidopsis thaliana*. *Plant Physiol* **93**, 907–914.
- 52 Passarinho PA & de Vries SC (2002) *Arabidopsis* Chitinases: a genomic survey. *Arabidopsis Book* **1**, e0023.
- 53 Kabir SR, Rahman MM, Tasnim S, Karim MR, Khatun N, Hasana I, Amin R, Islam SS, Nurujjaman M, Kabir AH *et al.* (2016) Purification and characterization of a novel chitinase from *Trichosanthes dioica* seed with antifungal activity. *Int J Biol Macromol* **84**, 62–68.
- 54 Zhang JZ, Kopparapu NK, Yan QJ, Yang SQ & Jiang ZQ (2013) Purification and characterisation of a novel chitinase from persimmon (*Diospyros kaki*) with antifungal activity. *Food Chem* **138**, 1225–1232.
- 55 Ano A, Takayanagi T, Uchibori T, Okuda T & Yokotsuka K (2003) Characterization of a class III chitinase from *Vitis vinifera* cv. Koshu. *J Biosci Bioeng* **95**, 645–647.
- 56 Chen YT, Hsu LH, Huang IP, Tsai TC, Lee GC & Shaw JF (2007) Gene cloning and characterization of a novel recombinant antifungal chitinase from papaya (*Carica papaya*). *J Agric Food Chem* **55**, 714–722.
- 57 Wang SY, Ye XY, Chen J & Rao PF (2012) A novel chitinase isolated from *Vicia faba* and its antifungal activity. *Food Res Int* **45**, 116–122.
- 58 Moore KG, Price MS, Boston RS, Weissinger AK & Payne GA (2004) A chitinase from Tex6 maize kernels inhibits growth of *Aspergillus flavus*. *Phytopathology* **94**, 82–87.
- 59 Wang SY, Shao B, Fu H & Rao PF (2009) Isolation of a thermostable legume chitinase and study on the antifungal activity. *Appl Microbiol Biotechnol* **85**, 313–321.
- 60 Truong NH, Park SM, Nishizawa Y, Watanabe T, Sasaki T & Itoh Y (2003) Structure, heterologous expression, and properties of rice (*Oryza sativa* L.) family 19 chitinases. *Biosci Biotechnol Biochem* **67**, 1063–1070.
- 61 Ohnuma T, Umemoto N, Taira T, Fukamizo T & Numata T (2013) Crystallization and preliminary X-ray diffraction analysis of an active-site mutant of ‘loopless’

- family GH19 chitinase from *Bryum coronatum* in a complex with chitotetraose. *Acta Crystallogr F* **69**, 1360–1362.
- 62 Ubhayasekera W, Tang CM, Ho SWT, Berglund G, Bergfors T, Chye ML & Mowbray SL (2007) Crystal structures of a family 19 chitinase from *Brassica juncea* show flexibility of binding cleft loops. *FEBS J* **274**, 3695–3703.
- 63 Putnam CD, Hammel M, Hura GL & Tainer JA (2007) X-ray solution scattering (SAXS) combined with crystallography and computation: defining accurate macromolecular structures, conformations and assemblies in solution. *Q Rev Biophys* **40**, 191–285.
- 64 Ohnuma T, Taira T, Umemoto N, Kitaoku Y, Sorlie M, Numata T & Fukamizo T (2017) Crystal structure and thermodynamic dissection of chitin oligosaccharide binding to the LysM module of chitinase-A from *Pteris ryukyuensis*. *Biochem Biophys Res Commun* **494**, 736–741.
- 65 Prasannath K (2017) Plant defense-related enzymes against pathogens: a review. *AGRIEAST J Agric Sci* **11**, 38–48.
- 66 Toufiq N, Tabassum B, Bhatti MU, Khan A, Tariq M, Shahid N, Nasir IA & Husnain T (2018) Improved antifungal activity of barley derived chitinase I gene that overexpress a 32 kDa recombinant chitinase in *Escherichia coli* host. *Braz J Microbiol* **49**, 414–421.
- 67 Rodrigues CHM, Pires DEV & Ascher DB (2018) DynaMut: predicting the impact of mutations on protein conformation, flexibility and stability. *Nucleic Acids Res* **46**, W350–W355.
- 68 Gross SM, Martin JA, Simpson J, Abraham-Juarez MJ, Wang Z & Visel A (2013) De novo transcriptome assembly of drought tolerant CAM plants, Agave deserti and *Agave tequilana*. *BMC Genom* **14**, 563.
- 69 Blommel PG & Fox BG (2007) A combined approach to improving large-scale production of tobacco etch virus protease. *Protein Expr Purif* **55**, 53–68.
- 70 Stols L, Gu MY, Dieckman L, Raffin R, Collart FR & Donnelly MI (2002) A new vector for high-throughput, ligation-independent cloning encoding a tobacco etch virus protease cleavage site. *Protein Expr Purif* **25**, 8–15.
- 71 Laemmli UK (1970) Cleavage of structural proteins during assembly of head of bacteriophage-T4. *Nature* **227**, 680–685.
- 72 Micsonai A, Wien F, Kernya L, Lee YH, Goto Y, Refregiers M & Kardos J (2015) Accurate secondary structure prediction and fold recognition for circular dichroism spectroscopy. *Proc Natl Acad Sci USA* **112**, E3095–E3103.
- 73 Lavinder JJ, Hari SB, Sullivan BJ & Magliery TJ (2009) High-throughput thermal scanning: a general, rapid dye-binding thermal shift screen for protein engineering. *J Am Chem Soc* **131**, 3794–3795.
- 74 Khan MA, Hamid R, Ahmad M, Abdin MZ & Javed S (2010) Optimization of culture media for enhanced chitinase production from a novel strain of *Stenotrophomonas maltophilia* using response surface methodology. *J Microbiol Biotechnol* **20**, 1597–1602.
- 75 Miller GL (1959) Use of dinitrosalicylic acid reagent for determination of reducing sugar. *Anal Chem* **31**, 426–428.
- 76 Franke D, Petoukhov MV, Konarev PV, Panjkovich A, Tuukkanen A, Mertens HDT, Kikhney AG, Hajizadeh NR, Franklin JM, Jeffries CM *et al.* (2017) ATSAS 2.8: a comprehensive data analysis suite for small-angle scattering from macromolecular solutions. *J Appl Crystallogr* **50**, 1212–1225.
- 77 Konarev PV, Volkov VV, Sokolova AV, Koch MHJ & Svergun DI (2003) PRIMUS: a Windows PC-based system for small-angle scattering data analysis. *J Appl Crystallogr* **36**, 1277–1282.
- 78 Svergun DI (1992) Determination of the regularization parameter in indirect-transform methods using perceptual criteria. *J Appl Crystallogr* **25**, 495–503.
- 79 Pettersen EF, Goddard TD, Huang CC, Couch GS, Greenblatt DM, Meng EC & Ferrin TE (2004) UCSF chimera – a visualization system for exploratory research and analysis. *J Comput Chem* **25**, 1605–1612.
- 80 Morris GM, Huey R, Lindstrom W, Sanner MF, Belew RK, Goodsell DS & Olson AJ (2009) AutoDock4 and AutoDockTools4: automated docking with selective receptor flexibility. *J Comput Chem* **30**, 2785–2791.

Supporting information

Additional supporting information may be found online in the Supporting Information section at the end of the article.

Fig. S1. PSI-Blast amino acid sequence alignment of the assembled ChiA1 from short reads of the transcriptome of *Agave tequilana* with seven chitinasas with the higher sequence identity.

Fig. S2. Activity of AtChi1 (yellow) and AtChi2 (purple) over insoluble colloidal chitin compared with the activity over the oligosaccharides chitohexaose (GlnNac)₆ and chitotriose (GlnNac)₃, under the same conditions (50 mM acetate buffer pH 5.0, 37 °C, 24 h) (see methodology).

Fig. S3. A superposition of the five CatD Robetta models, which gave very small differences.

Fig. S4. Binding poses of chitohexaose for the docking simulations of the five CatDs Robetta models.